Probing many-body quantum states in single InAs quantum dots: Terahertz and tunneling spectroscopy

Y. Zhang,[1,*] K. Shibata,[1,2,†] N. Nagai,[1] C. Ndebeka-Bandou,[1,3] G. Bastard,[1,3] and K. Hirakawa[1,2,‡]

[1]*Center for Photonics Electronics Convergence, Institute of Industrial Science, University of Tokyo, 4-6-1 Komaba, Meguro-ku, Tokyo 153-8505, Japan*

[2]*Institute for Nano Quantum Information Electronics, University of Tokyo, 4-6-1 Komaba, Meguro-ku, Tokyo 153-8505, Japan*

[3]*Laboratoire Pierre Aigrain, Ecole Normale Superieure, 24 rue Lhomond, F-75005 Paris, France*

We have investigated the many-body quantum states in single InAs quantum dots (QDs) by simultaneously obtaining the terahertz (THz) intersublevel transition and single electron tunneling spectra. It is found that the intersublevel transition energies measured in the few-electron region are systematically larger than the excited state (ES) energies determined from the transport measurements. We show that tunneling and THz spectroscopy probe the same many-body excited states in the QDs, but their sensitivities depend on their selection rules. In the many-electron region, we observe THz peaks whose energies coincide with the tunneling ESs.

Self-assembled InAs quantum dots (QDs) are very attractive materials owing to the discrete nature of their low lying electronic spectrum [1]. This reminiscence of the atomic energy levels has often led people to term these QDs "artificial atoms." The QD size being comparable to the effective Bohr radius implies that the electrical and optical properties of InAs QDs are strongly affected by many-body effects. Since typical energy separations for the zero-dimensional sublevels in the InAs QDs are 10–100 meV and in the same order with the magnitude of electron-electron (el-el) interactions, an understanding of many-body effects on sublevel structures is crucial, particularly for device applications that utilize intersublevel transitions.

To investigate the sublevel structures in InAs QDs, available techniques are rather limited. Terahertz (THz) intersublevel transition spectroscopy was initially performed on an ensemble of QDs [2,3] and, more recently, on single QDs by utilizing the scanning probe microscope technique [4–6]. However, due to the broad linewidth and low signal-to-noise (S/N) ratios, a detailed discussion on the many-body states was not possible. Another way to probe the electronic states in QDs is by single electron tunneling spectroscopy [7–10]. However, it is considered that there is an intrinsic difference between the two types of measurements. In THz spectroscopy, the excited states (ESs) are probed by optically exciting an electron from the ground state (GS). Since such photoexcitation inevitably affects other electrons in the QD, the transition energy is strongly modulated by el-el interactions, giving rise to many-body corrections such as the excitonic effect and depolarization effect [11,12]. However, in transport measurements, the ESs are probed by introducing an electron in the QD from an electrode. It is crucial to clarify the relationship between THz and single electron tunneling spectroscopy to understand the many-body electronic states in QDs, and a systematic comparison between the two types of measurements is therefore highly desirable.

In this Rapid Communication, we discuss the many-body quantum states in single InAs QDs by simultaneously obtaining THz intersublevel transition spectra [13] and tunneling spectroscopy data. We used a single electron transistor (SET) geometry [14] that consisted of an InAs QD and nanogap metal electrodes and detected the intersublevel transitions by measuring a photocurrent induced in the SET. By doing so, we are able to obtain THz intersublevel transition spectra of a high S/N ratio that can be compared with transport data and make a systematic comparison between the two types of measurements. We have found that the intersublevel transition energies measured in the few-electron region are systematically larger than the ES energies determined from transport measurements. We will show that this is because the transport and THz spectroscopy probe the same many-body ESs in the QDs, but with different sensitivities. When the many-body wave functions have complex wave-function patterns in the many-electron region, we indeed observe the ESs whose energies coincide with the THz peaks.

The self-assembled InAs QDs were grown by molecular beam epitaxy on semi-insulating GaAs substrates. After successively growing a 300-nm-thick Si-doped GaAs layer, a 100-nm-thick undoped $Al_0.3Ga_0.7$ As barrier layer, and a 200-nm-thick undoped GaAs buffer layer, self-assembled InAs QDs were grown by depositing four monolayers of InAs at 480–490 °C, as shown in Fig. 1(a). We used quasicircular QDs with a diameter of ∼90 nm grown on a (100)-oriented substrate for the study in the few-electron region. The sample used for the many-electron region was grown on a (211)B-oriented substrate. On the (211)B surfaces, the QDs are elongated in the [011] direction [15,16]. Hereafter, we call these elongated quantum dots "quantum dashes" (QDHs). The large size of the QDHs is suitable for accommodating many electrons and also for obtaining a high tunnel conductance (∼1 μS) required for THz photocurrent measurements [13]. The size of the InAs QDH used in this study was $130x60nm^2$. A pair of Ti(5 nm)/Au(15 nm) electrodes separated by a 20–40 nm gap were directly deposited on the QDs/QDHs and used as the source and drain electrodes. The gate voltage V_G was applied to the Si-doped GaAs buffer layer to change the electrostatic potential in the QDs/QDHs. Coulomb stability diagrams were

---

*Electronic mail: zhangya@iis.u-tokyo.ac.jp

†Permanent address: Department of Electronics and Intelligent Systems, Tohoku Institute of Technology, Sendai 982-8577, Japan.
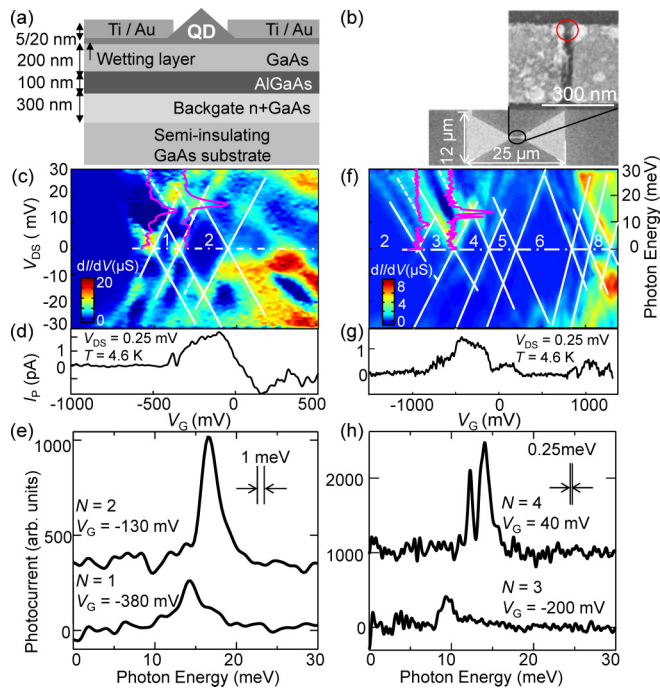
‡Electronic mail: hirakawa@iis.u-tokyo.ac.jp

FIG. 1. (Color online) (a) Cross section of the QD-SET sample. (b) SEM images of QD-SET A with a bowtie antenna structure. The QD is marked by a red circle. (c) Coulomb stability diagram of QD-SET A. White solid lines are guides to the eye for the boundaries of Coulomb diamonds. White dashed lines denote the ESs. The numbers in the Coulomb diamonds denote the number of electrons in the dot. Pink curves are the photocurrent spectra. (d) THz-induced photocurrent as a function of V_G measured on QD-SET A by applying a small source-drain voltage ($V_{DS} = 0.25$ mV). (e) Photocurrent spectra measured at various V_G on QD-SET A. (f) Coulomb stability diagram of QD-SET B. Pink curves are the photocurrent spectra. (g) THz-induced photocurrent as a function of V_G measured on QD-SET B. (h) Photocurrent spectra measured at various V_G on the QD-SET B.

measured by sweeping the back-gate voltage V_G. All the measurements were performed at 4.6 K.

Figure 1(b) shows a scanning electron microscope (SEM) image of a QD-SET sample (QD-SET A). A bowtie antenna was integrated with the nanogap electrodes [17]. From the SEM image, the QD is slightly elongated ($\sim$10%) along the direction of the nanogap electrodes, as shown in the inset of Fig. 1(b). Figure 1(c) shows the Coulomb stability diagram of the fabricated QD-SET. The numbers shown in the Coulomb diamonds denote the number of electrons in the QD, N. From the stability diagram, we can determine the charging energy E_C to be around 10 meV. Furthermore, when $N = 1$, an ES line touches the diamond from the upper left side (dashed line) and we can determine the ES energy to be 14.3 ± 1 meV. Similarly, when $N = 2$, the ES (dashed line) is observed at around 11.2 ± 1 meV above the GS.

The light source used in this experiment was a SiC globar placed in a Fourier transform spectrometer (FTS) and provided broadband blackbody THz radiation. Figure 1(d) shows the photocurrent induced by the THz radiation measured as a function of V_G by applying a small source-drain voltage ($V_{DS} = 0.25$ mV). The photocurrent was $\sim$1 pA. By using the
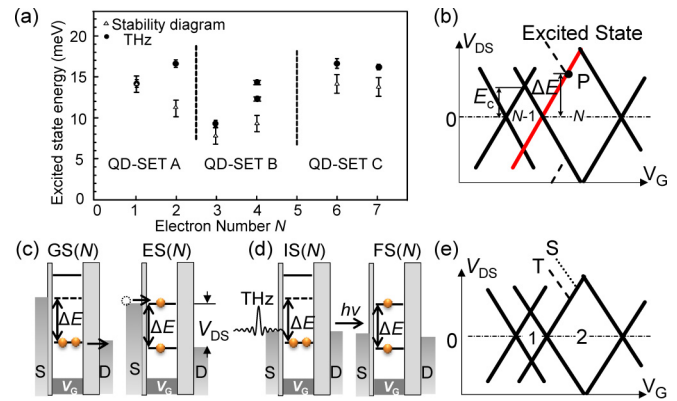

FIG. 2. (Color online) (a) Excited state (ES) energies determined from the transport measurements (triangles) and the THz measurements (circles) are plotted as a function of the electron number N. The data were summarized for three QD-SETs. (b) Schematic illustration of a Coulomb stability diagram that shows ES lines (dashed lines). The height of point P expresses the ES energy. (c) Energy band diagram for the ES spectroscopy in the tunneling measurement. (d) Energy band diagram for the THz intersublevel transition spectroscopy. (e) Schematic Coulomb stability diagram for electron numbers $N = 1$ and 2. Two ESs (triplet and singlet) are shown by a dashed line and a dotted line, respectively. The triplet ES (T) tends to be more visible than the singlet ES (S) in the stability diagram, whereas the THz spectra measure only the singlet ES.

FTS, we were able to obtain the THz-induced photocurrent spectra, corresponding to the intersublevel transition spectra in the QD [13]. We could perform the spectral measurements only in the Coulomb blockaded regions, because the shot noise was very large in the single electron tunneling regions. Figure 1(e) shows the photocurrent spectra measured at two different V_G. When $N = 1$, a photocurrent peak was observed at 14.3 meV, which agrees well with the ES energy determined from the stability diagram. When $N = 2$, a photocurrent peak was observed at 16.7 meV. However, this photon energy is significantly larger than the ES energy obtained from the stability diagram (11.2 ± 1 meV).

A similar behavior was observed in another QD-SET (QD-SET B), whose stability diagram and measured photocurrent are plotted in Figs. 1(f) and 1(g), respectively. We observed THz-induced photocurrent in the $N = 3$ and 4 Coulomb diamonds. Figure 1(h) shows the photocurrent spectra measured for $N = 3$ and 4. When $N = 3$, an ES (the dashed line in the stability diagram) was observed at 7.8 ± 1 meV, whereas the measured photocurrent peak was located at 9.8 meV. Similarly, when $N = 4$, a transport ES was observed at 9.3 ± 1 meV, whereas the measured photocurrent peaks were at 12–14 meV. For easier comparison, we plotted the THz spectra on the Coulomb stability diagrams in Figs. 1(c) and 1(f).

Figure 2(a) summarizes the ES energies determined from the THz and transport measurements for the QD-SETs in the few-electron region. As seen in the figure, the ES energy determined from the transport agrees with the THz data only when $N = 1$. When $N > 1$, the THz photon energies are systematically larger than the ES energies determined from transport data. One may think this difference is reasonable, since it is known that the intersublevel transition spectra are

affected by many-body corrections [11,12]. However, this naive explanation falls short of being conclusive, as we show below.

To understand the difference between the THz and transport measurements, let us examine what we really measure by the two methods. Figure 2(b) shows a schematic illustration of a Coulomb stability diagram that shows an ES line (dashed line). Figure 2(c) illustrates the band diagram for the bias point P in Fig. 2(b). It is known that the electrochemical potential difference eV_{DS} at point P in the stability diagram is exactly equal to the total energy difference between the GS and the ES [18],

$$U_{ES}(N) - U_{GS}(N) = eV_{DS}. \quad (1)$$

Figure 2(d) illustrates the energy band diagram for the initial state (IS) and the final state (FS) for the THz measurement. When an optical transition takes place between the IS and the FS, the absorbed photon energy must be equal to the total energy difference between the IS and FS in order to fulfill the energy conservation,

$$U_{FS}(N) - U_{IS}(N) = h\nu, \quad (2)$$

where $h\nu$ is the absorbed THz photon energy.

As shown in Figs. 2(c) and 2(d), the electronic structures in the QD for the GS and ES in transport measurements are identical with those for the IS and FS in THz spectroscopy, respectively; the difference lies only in the external voltages V_{DS} and V_G applied to the QD-SET. Now, if the coupling between the QD and electrodes is weak, which is evidenced by the straight boundaries of the Coulomb stability diagram, Eqs. (1) and (2) indicate that the ES energies determined from the transport and the intersublevel transition energy $h\nu$ should match with each other. However, Fig. 2(a) shows that this is apparently not the case.

Here, we would like to emphasize that the Coulomb stability diagrams and THz spectra probe the same many-body states, but with different sensitivities. Let us consider the simplest many-electron case, i.e., $N = 2$. The ESs of the two electrons can be either in a spin singlet or a triplet state [19]. The orbital parts of their wave function are symmetrical (singlet) or antisymmetrical (triplet) in the exchange of the two electrons. The different configurations give different Coulomb repulsion energies; the singlet ES (dotted line) has a higher energy than the triplet ES (dashed line), as illustrated in Fig. 2(e). For the GS, however, only the spin singlet exists. When the QD is optically excited, the spin configuration is conserved and hence only the singlet → singlet transition is allowed.

On the other hand, no such spin selection rule restricts the transport. Therefore, when we gradually increase the source-drain voltage V_{DS}, the triplet ES is detected first and shows up as the ES in the stability diagram. Note here that since the Coulomb stability diagram plots the differential conductance dI/dV, only the ESs that significantly increase the tunneling current appear clearly. Since the singlet and triplet ESs have similar orbital wave functions in the few-electron regions, their tunnel conductances are also similar. As V_{DS} is further increased, the singlet ES enters the bias window. However, the singlet state cannot increase the tunneling current as large as the triplet state does, because an electron tunnels via only one of the transport channels (singlet *or* triplet)
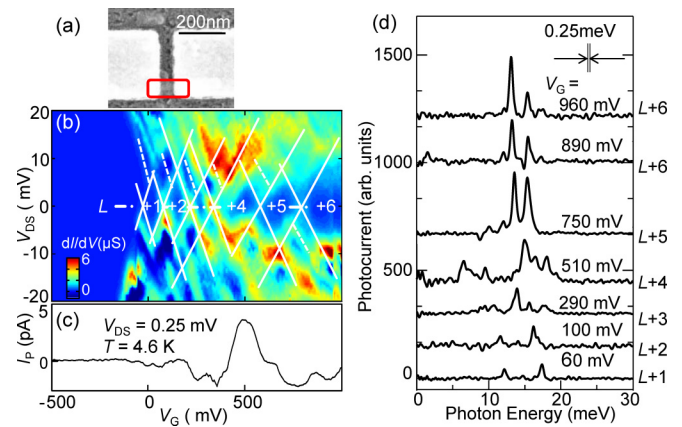

FIG. 3. (Color online) (a) A SEM image of a QDH-SET sample. The QDH is marked by a red rectangle. (b) A Coulomb stability diagram of the QDH-SET. The numbers in the figure $(L, L+1, L+2, \ldots)$ denote the numbers of electrons in the QDH. (c) THz-induced photocurrent as a function of V_G measured at $V_{DS} = 0.25$ mV. (d) Photocurrent spectra measured at various V_G on the QDH-SET with $V_{DS} = 0.25$ mV.

in the single electron tunneling process. Therefore, the ES with the lower energy is more visible in the stability diagram and the ES energies determined by the THz spectroscopy are systematically larger than those determined from the Coulomb stability diagrams. From the measurements for $N = 2$ [see Fig. 2(a)], we could determine that the energy difference between the singlet and triplet is 5.5 ± 1 meV.

The above discussion addressed the two-electron case. With an increasing electron number, the many-body wave functions become more complex and we have more chances of finding ESs that can be probed by both THz and tunneling spectroscopy. To see this, we performed measurements on a QDH sample that works in the many-electron region. Figure 3(a) shows an SEM image of a QDH sample. The Coulomb stability diagram of the QDH-SET is shown in Fig. 3(b). The numbers shown in the diamonds denote the number of electrons in the QDH, N [20,21]. For $N > L$ (L denotes the electron number in the large Coulomb diamond at the left end), the addition energy $E_a(N)$ is smaller than 10 meV and the orbital energy difference ΔE is estimated to be 3–5 meV.

Figure 3(c) shows the photocurrent measured as a function of V_G by applying a small source-drain voltage ($V_{DS} = 0.25$ mV). The photocurrent spectra measured at various V_G are plotted in Fig. 3(d). Multiple sharp photocurrent peaks are observed at around 15 meV. However, these photon energies are much larger than the low lying ES energies determined from the Coulomb stability diagram [typically 3–5 meV; see the white dashed lines in Fig. 3(a)], as in the few-electron region.

To examine even higher excited states, we plotted the THz spectra on the Coulomb stability diagrams in Fig. 4(a) and compared the THz peak energies with the ES energies in the transport data. The white solid lines and the black dashed lines are guides to the eye for the GSs and ESs, respectively. The curves in pink are the THz photocurrent spectra, and the numbers shown above the spectra denote the
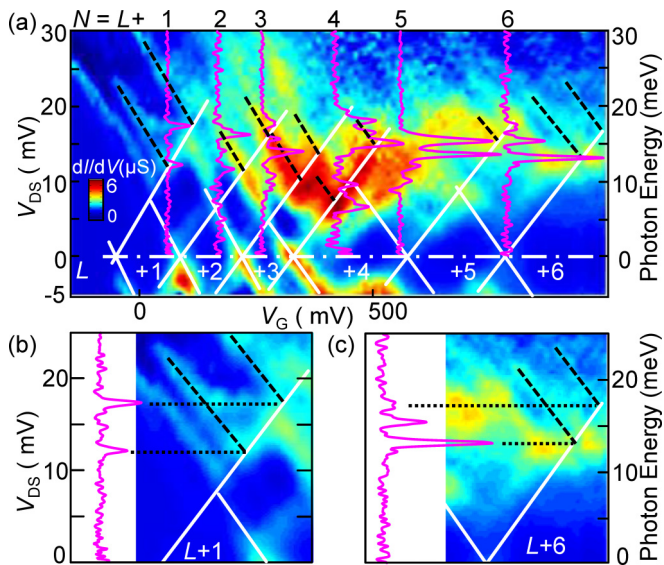
FIG. 4. (Color online) (a) The THz spectra and the Coulomb stability diagram for QDH-SET. Pink curves are the photocurrent spectra and the numbers shown above the spectra denote the electron numbers in the QD. The black dashed lines show the ESs that have the same excitation energies with the THz photocurrent peaks. (b) and (c) show the THz spectra and the Coulomb stability diagrams for $N = L + 1$ and $L + 6$, respectively. The dotted lines indicate the photocurrent peaks that have the same energy as the transport ESs.

number of electrons in the QDH [22]. Surprisingly, we can find the transport ESs whose energies coincide with those of the photocurrent peaks. In Figs. 4(b) and 4(c), we show blowups of the transport and THz data for $N = L + 1$ and $L + 6$, respectively. The dotted lines indicate the transport ESs that have the same energies with the photocurrent peaks. When $N = L + 4$, bunched photocurrent peaks are observed around $V_{DS} = 7$ and 15 meV. Around these V_{DS}'s, we can see broad conductance peaks in the Coulomb stability diagram, although the individual conductance peaks cannot be resolved due to finite temperature in the transport measurement. The agreement confirms that both the THz intersublevel transition spectroscopy and the single electron tunneling spectroscopy basically probe the same many-body ESs.

Finally, we would like to make a comment on the many-body corrections to the intersublevel transition spectra. Many-body corrections such as the excitonic effects and depolarization effects [11,12] have been introduced to account for the difference between the measured intersublevel (intersubband) transition energies and the single-particle sublevel (subband) energy separations. However, we would like to emphasize that both THz spectroscopy and single electron tunneling spectroscopy are affected by many-body corrections by the same magnitude, which can be understood by comparing Figs. 2(c) and 2(d). Therefore, the difference observed between the single electron tunneling spectroscopy and the THz spectroscopy is not due to the difference in many-body corrections, but due to their selection rules.

In summary, we have investigated the many-body quantum states in single self-assembled InAs QDs by measuring the THz-induced photocurrent. It is found that the intersublevel transition energies are systematically larger than the ES energies determined from single electron tunneling measurements. This is associated with the fact that the intersublevel transition takes place only between the GS and the collective ESs allowed by the optical selection rule, whereas the lowest ES is more visible in the Coulomb stability diagrams. In the many-electron region, we could indeed identify multiple ESs whose energies agree with the THz peaks. This work has presented a systematic comparison between tunneling and THz spectroscopy data on zero-dimensional electron systems and clarified the relationship between the information on the many-body electronic states obtained by the two dissimilar measurements.

[1] P. M. Petroff, A. Lorke, and A. Imamoglu, Phys. Today **54**(4), 46 (2001).

[2] H. Drexler, D. Leonard, W. Hansen, J. P. Kotthaus, and P. M. Petroff, Phys. Rev. Lett. **73**, 2252 (1994).

[3] S. Hameau, Y. Guldner, O. Verzelen, R. Ferreira, G. Bastard, J. Zeman, A. Lemaitre, and J. M. Gerard, Phys. Rev. Lett. **83**, 4152 (1999).

[4] J. Houel, S. Sauvage, P. Boucaud, A. Dazzi, R. Prazeres, F. Glotin, J.-M. Ortéga, A. Miard, and A. Lemaître, Phys. Rev. Lett. **99**, 217404 (2007).

[5] S. Sauvage, A. Driss, F. Réveret, P. Boucaud, A. Dazzi, R. Prazeres, F. Glotin, J.-M. Ortéga, A. Miard, Y. Halioua, F. Raineri, I. Sagnes, and A. Lemaître, Phys. Rev. B **83**, 035302 (2011).

[6] R. Jacob, S. Winnerl, M. Fehrenbacher, J. Bhattacharyya, H. Schneider, M. T. Wenzel, H-G. Ribbeck, L. M. Eng, P. Atkinson, O. G. Schmidt, and M. Helm, Nano Lett. **12**, 4336 (2012).

[7] L. P. Kouwenhoven, T. H. Oosterkamp, M. W. S. Danoesastro, M. Eto, D. G. Austing, T. Honda, and S. Tarucha, Science **278**, 1788 (1997).

[8] S. Tarucha, D. G. Austing, Y. Tokura, W. G. van der Wiel, and L. P. Kouwenhoven, Phys. Rev. Lett. **84**, 2485 (2000).

[9] D. M. Zumbühl, C. M. Marcus, M. P. Hanson, and A. C. Gossard, Phys. Rev. Lett. **93**, 256801 (2004).

[10] S. M. Reimann and M. Manninen, Rev. Mod. Phys. **74**, 1283 (2002).

[11] S. J. Allen, Jr., D. C. Tsui, and B. Vinter, Solid State Commun. **20**, 425 (1976).

[12] T. Ando, A. B. Fowler, and F. Stern, Rev. Mod. Phys. **54**, 437 (1982).

[13] Y. Zhang, K. Shibata, N. Nagai, C. Ndebeka-Bandou, G. Bastard, and K. Hirakawa, Nano Lett. **15**, 1166 (2015).

[14] M. Jung, T. Machida, K. Hirakawa, S. Komiyama, T.Nakaoka, S. Ishida, and Y. Arakawa, Appl. Phys. Lett. **87**, 203109 (2005).

[15] K. Shibata, K. Seki, P. Luukko, E. Räsänen, K. M. Cha, I. Horiuchi, and K. Hirakawa, Appl. Phys. Lett. **99**, 182104 (2011).

[16] K. Shibata, N. Pascher, P. J. J. Luukko, E. Räsänen, S. Schnez, T. Ihn, K. Ensslin, and K. Hirakawa, Appl. Phys. Express **7**, 045001 (2014).

[17] K. Shibata, A. Umeno, K. M. Cha, and K. Hirakawa, Phys. Rev. Lett. **109**, 077401 (2012).

[18] R. Hanson, L. P. Kouwenhoven, J. R. Petta, S. Tarucha, and L. M. K. Vandersypen, Rev. Mod. Phys. **79**, 1217 (2007).

[19] The three triplet ESs have the same energy since they have the same orbital wave functions. Therefore, we describe them as one triplet ES in the analysis.

[20] Although L could not be determined from the experiment performed in this work, L is larger than 0, because Coulomb diamonds could be seen even for more negative V_G region in another measurement [21]. Therefore, the QDH-SET is in the many-electron region.

[21] See Supplemental Material at http://link.aps.org/supplemental/10.1103/PhysRevB.91.241301 for the electron number in the QDH-SET.

[22] Due to the asymmetric tunneling barriers of the sample, the Coulomb stability diagram exhibits more features on the positive bias side. Therefore, we compare the THz spectra with the ESs in the Coulomb stability diagram for $V_{DS} > 0$.